

Supporting Information:

**Highly efficient and stable indium monatomic catalyst for
electrocatalytic reduction of CO₂ to formate**

Dafu Xu, Yan Xu, Haixia Wang, Xiaoqing Qiu*

College of Chemistry and Chemical Engineering, Central South University, Changsha, Hunan

410083, P. R. China

Email: xq-qiu@csu.edu.cn

Contents

Experiment section

Figures

Fig. S1. XRD patterns of ZIF-8 (a), and In doped ZIF-8 with In/Zn mole ratio of 1:9 (b) and 2:8 (c)

Fig. S2. XRD patterns of NC, In-SACs (a) and In @NC (b).

Fig. S3. STEM images of In @NC.

Fig. S4. XPS spectra for the survey scan of NC, In-SACs and In @NC.

Fig. S5. XPS spectra for the N 1s region of In @NC.

Fig. S6. N₂ sorption isotherms (a) and the corresponding pore size distribution (b) of the In-SACs, In@NC and NC samples.

Fig. S7. Typical three-electrode H-type setup for the electrochemical ECR measurements.

Fig. S8. LSV curves of In-SACs in CO₂-saturated and Ar-saturated KHCO₃ solution.

Fig. S9. Representative NMR spectrum of the electrolyte after CO₂ reduction electrolysis at -1.31 V vs. RHE for In-SACs.

Fig. S10. The calibration curves of H₂, corresponding chromatographic peak.

Fig. S11. The calibration curves of CO, corresponding chromatographic peak.

Fig. S12. FEs of CO, H₂ and HCOO⁻ for In @NC.

Fig. S13. Electrochemical capacitance measurements of (a) In-SACs, (b) In @NC, (c)

NC with different scan rate. (d) Linear fittings of the current density differences (ΔJ) with the scan rates to determine the double layer capacitance (C_{dl}) and electrochemical surface area (ECSA).

Fig. S14. (a) Nyquist plots for In-SACs, In @NC and NC. (b) Tafel plots of the partial HCOO^- current density for In-SACs and In @NC at different potentials.

Fig. S15. XPS In 3d spectra of In-SACs obtained before and after electrochemical reduction.

Tables

Table S1. Comparison of electrocatalytic property in literatures.

1. Experimental Section

1.1 Materials

Indium nitrate hydrate (99%, Aladdin), zinc nitrate hexahydrate (98%, Aladdin), 2-methylimidazole (Aladdin), methanol (Sinopharm Chemical), ethanol (Sinopharm Chemical), KHCO_3 (99.5%, Innochem) were used without any further purification.

1.2 Synthesis of catalyst

Typically, 3.94 g of 2-methylimidazole (2-MeIm) was dissolved in 80 mL of methanol/ethanol solution (methanol: ethanol = 1:1) with stirring for 30 min (Solution A). Meanwhile, $\text{Zn}(\text{NO}_3)_2 \cdot 6\text{H}_2\text{O}$ (1.785g) and with a given amount of $\text{In}(\text{NO}_3)_3$ (In/Zn mole ratio was set to be 1:9 or 2:8) were dissolved in another 80 mL of methanol/ethanol solution (methanol : ethanol = 1:1) under stirring for 30 min (Solution B). Then, Solution B was added into Solution A under continuous stirring for 24 h at room temperature. The precipitate was separated by centrifugation, and washed with ethanol for several times, finally dried at 60 °C for 12 h under vacuum to obtain the In doped zeolitic imidazolate frameworks (ZIF-8) precursors. For comparison, parallel control experiments for pure ZIF-8 preparation were performed under identical condition except that no $\text{In}(\text{NO}_3)_3$ was added.

The precursor powder was subjected to a pyrolysis and carbonization process at 910 °C for 2 h in a tubular furnace under protection of flowing N_2 atmosphere to yield catalysts. The as-obtained samples were denoted as NC, In-SACs, and In@NC, according to the corresponding precursors of ZIF-8, In doped ZIF-8 with In/Zn mole ratio of 1:9 and 2:8, respectively.

1.3. Material characterization

X-ray diffraction (XRD) patterns were obtained from a D8 Advance diffractometer instrument equipped with $\text{Cu K}\alpha$ source (Bruker D8, 40 kV, 40 mA, with scan rate of 5°min^{-1} from 10 to 80°). The morphologies of the samples were analyzed with transmission electron microscope (TEM, FEI Tecnai G2 F20 S-Twin) and field-emission scanning electron microscope (FE-SEM). The surface atomic structure was shown by spherical-aberration-corrected TEM in a STEM mode with a high-angle annular dark-field (HAADF) detector (JEOL JEM-ARM200 F). The X-ray

photoelectron spectroscopy (XPS) results were recorded using a Phoibos 100 (SPECS) hemispherical electron analyzer. The Raman measurements were taken using a Renishaw spectrometer at 532 nm on a Renishaw Microscope System RM2000. X-ray absorption spectroscopy including x-ray absorption near edge spectra (EXAFS) and extended x-ray absorption fine structure (EXAFS) at In K-edge were performed on the beamline BL14W1 of National Synchrotron Light Source (SSLS) operated at 3.5 GeV with a constant current of 220 mA, equipped with a double Si (111) crystal monochromator. The XANES and EXAFS were processed using the Athena software package. The ICP-OES measurements were taken on an Agilent 5110 inductively coupled plasma optical emission spectrometry (ICP-OES) system.

1.4 Electrochemical CO₂RR measurements

1.4.1 Electrochemical measurements

All electrochemical measurements were carried out on a CHI 660e electrochemical workstation in a three-electrode configuration cell. The as-prepared electrode as the working electrode. Pt sheet electrode was used as the counter electrode and Ag/AgCl (saturate KCl) electrode was used as the reference electrode in 0.5 M KHCO₃ aqueous electrolyte. The electrode potential was converted to the RHE reference scale by the formula $E(\text{vs. RHE}) = E(\text{vs. Ag/AgCl}) + 0.21 \text{ V} + 0.0591 \times \text{pH}$. Nafion 117 membrane was inserted between the anodic chamber and anodic chamber of H-type cell. Before conducting the test, continuously feed Ar (gas) or CO₂ into the cathode compartment (constant rate) until saturation. Initially, The LSV curves were conducted at scan rate of 10 mV/s with always bubbling Ar or CO₂. CV measurements were performed under the potentials from 0 to 0.1 V at various scan rates in CO₂-saturated 0.5 M KHCO₃ in order to measure double layer capacitance (C_{dl}). Where C_{dl} corresponds to the slope of the double-layer charging current *versus* the scan rate plot. Then the electrochemical impedance spectra (EIS) tests were carried out under CO₂-saturated atmospheres.

1.4.2 CO₂ reduction experiments

Electrochemical CO₂ER was carried out in CO₂-saturated 0.5 M KHCO₃ solution. The potential range of electrolysis was -1.6 ~ -2.2 V vs. Ag/AgCl. After the electrolysis, Gas products from the cathode compartment were analyzed by using an online gas

chromatograph (GC) equipped with a BID detector and ShinCarbon ST100/120 packed column. Thermal conductivity detector for H₂, flame ionization detector for CO. The faradaic efficiencies of the gas products were calculated by using the concentrations (ppm) detected by GC as follows:

$$FE = \frac{nzF}{Q} = \frac{V\% vzF}{V_m I} \times 100\%$$

Where V% is the relative gas content read directly from the gas chromatograph; z is the number of electrons required for electrocatalytic reduction of CO₂ to CO; F is the Faraday constant (96485 C mol⁻¹) and V_m is the gas molar volume under standard conditions, V_m = 22.4 L mol⁻¹, I is the current. Quantitative analysis of liquid products after electrolysis using liquid-phase nuclear magnetic resonance (NMR) spectroscopy. The ¹H NMR spectroscopy was performed with a 500 MHz spectrometer (Bruker AVANCE III 500). The water suppress method was used. The intensity of the HCOOH peak was compared to the standard curve to quantify the concentration of HCOOH. The following was the equation for calculating the FE of liquid-phase products (HCOOH):

$$FE = \frac{n_{\text{formate}} z f}{Q_{\text{total}}} \times 100\%$$

Where n_{formate} is the measured amount of formate in the cathodic compartment and z is the number of electrons required for electrocatalytic reduction of CO₂ to HCOOH; the F is Faraday constant (96485 C mol⁻¹) and Q_{total} is total charge during the CO₂ER.

Figures

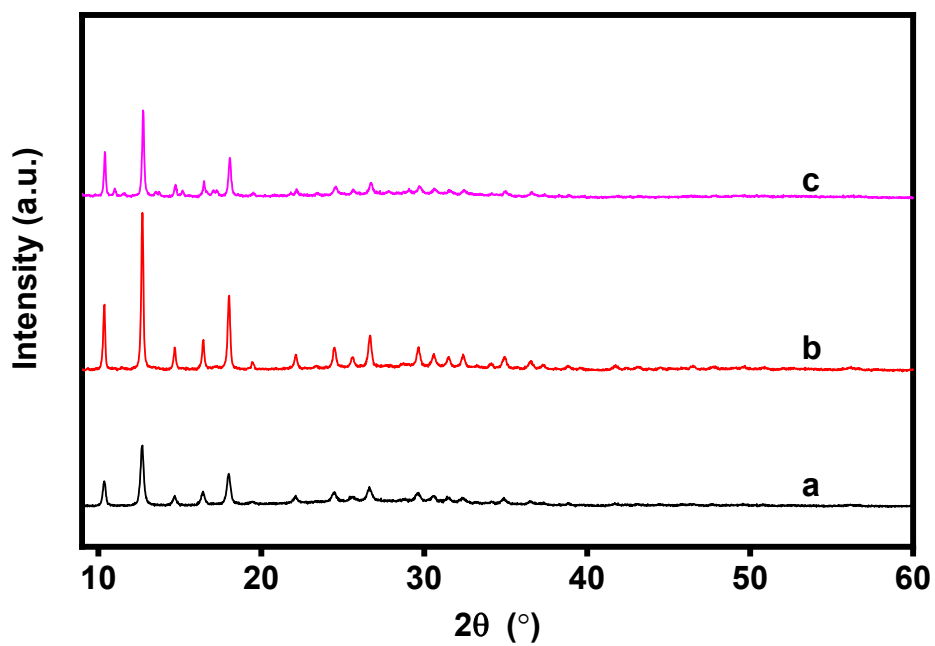


Fig. S1. (a) XRD patterns of ZIF-8 (a) and In doped ZIF-8 with In/Zn mole ratio of 1:9 (b) and 2:8 (c)

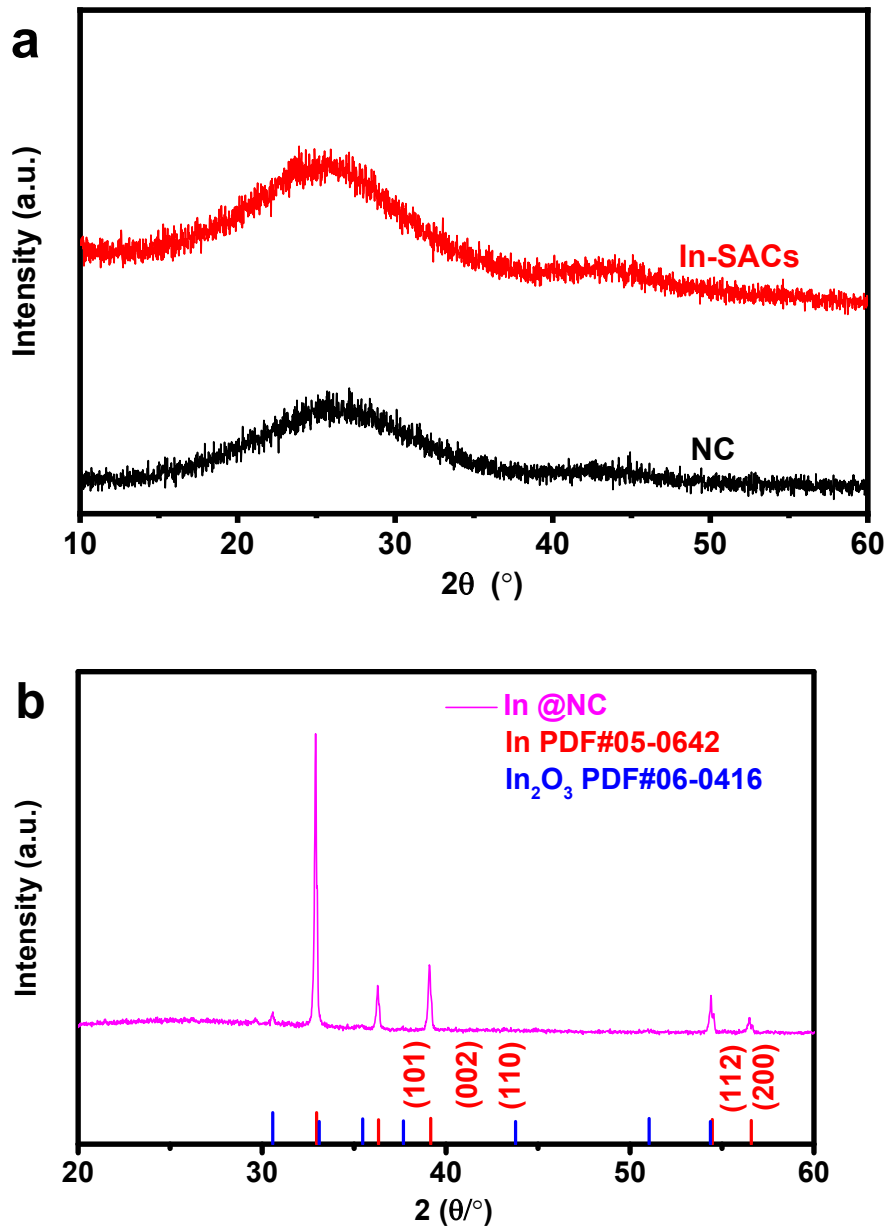


Fig. S2. XRD patterns of (a)NC and In-SACs, (b) In@NC

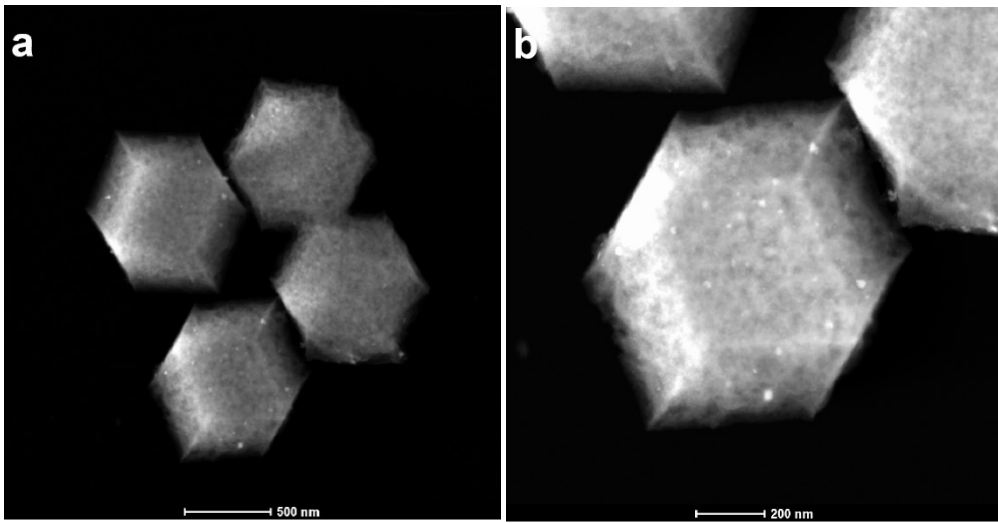


Fig. S3. STEM images of In@NC.

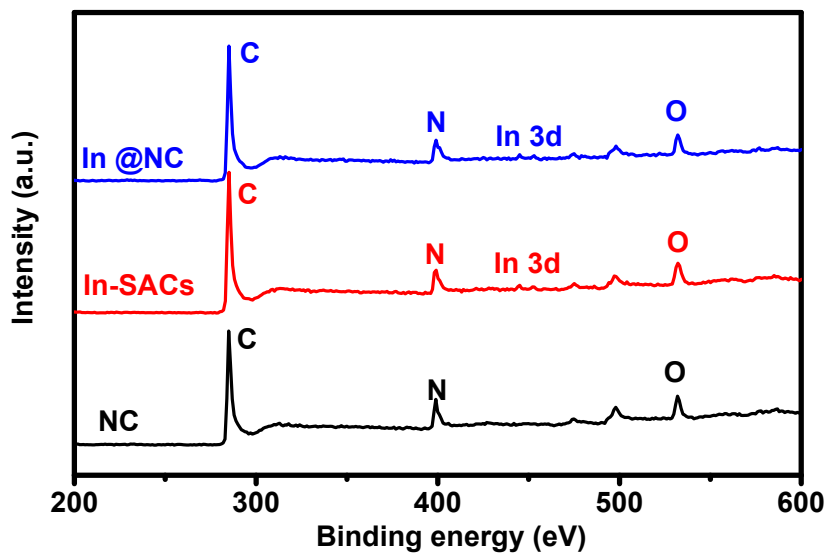


Fig. S4. XPS spectra for the survey scan of NC, In-SACs and In@NC.

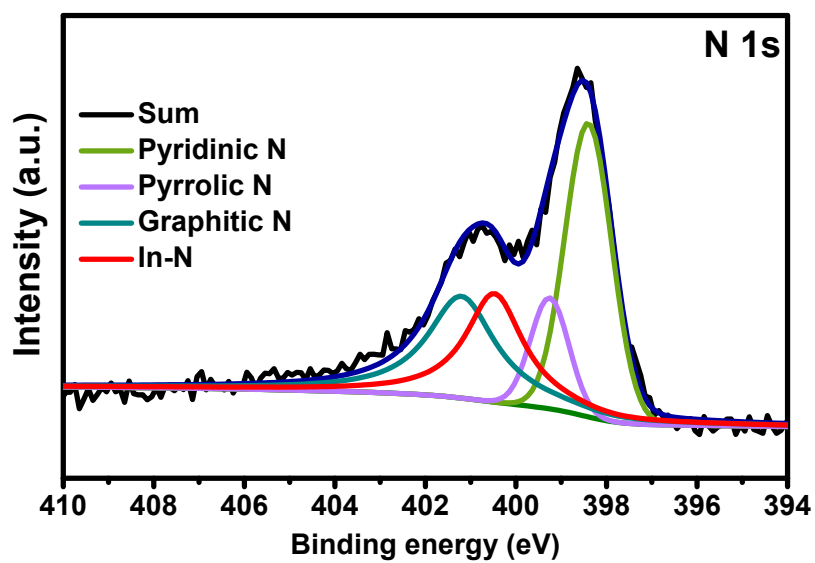


Fig. S5. XPS spectra for the N 1s region of In@NC.

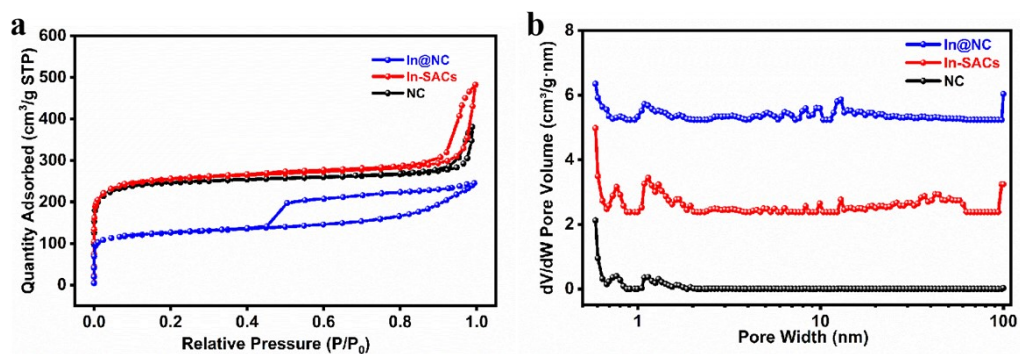


Fig. S6. N₂ sorption isotherms (a) and the corresponding pore size distribution (b) of the In-SACs, In@NC and NC samples.

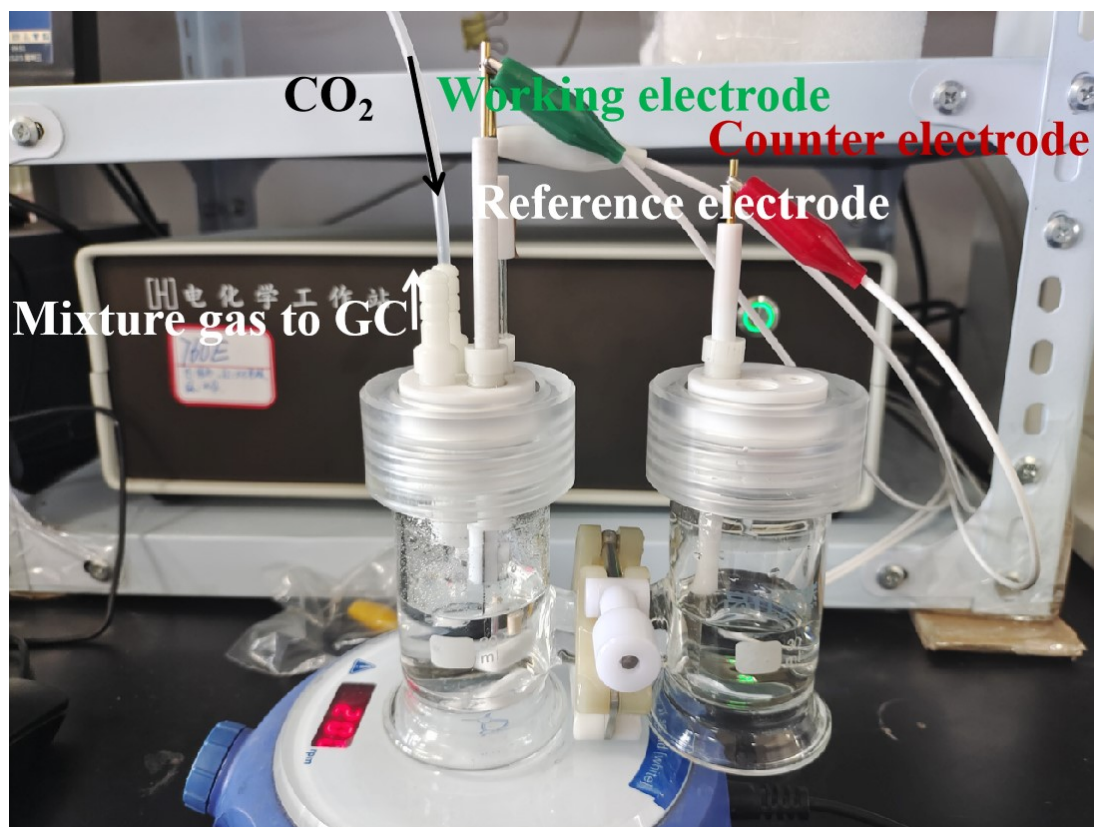


Fig. S7. Typical three-electrode H-type setup for the electrochemical ECR measurements.

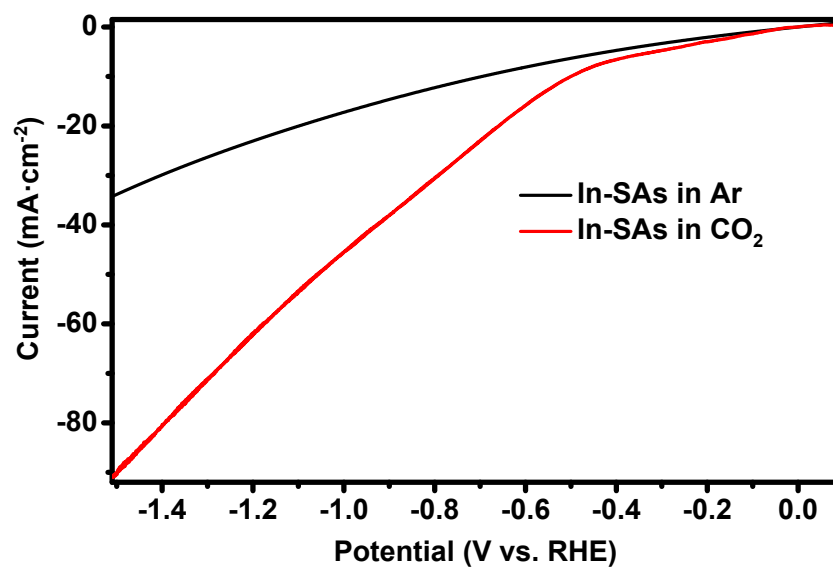


Fig. S8. LSV curves of In-SACs in CO₂-saturated and Ar-saturated KHCO₃ solution.

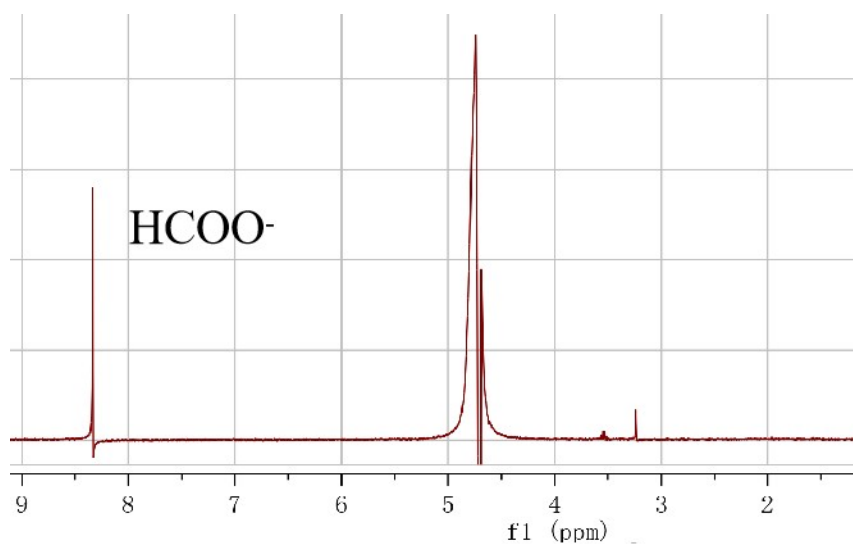


Fig. S9. Representative NMR spectrum of the electrolyte after CO₂ reduction electrolysis.

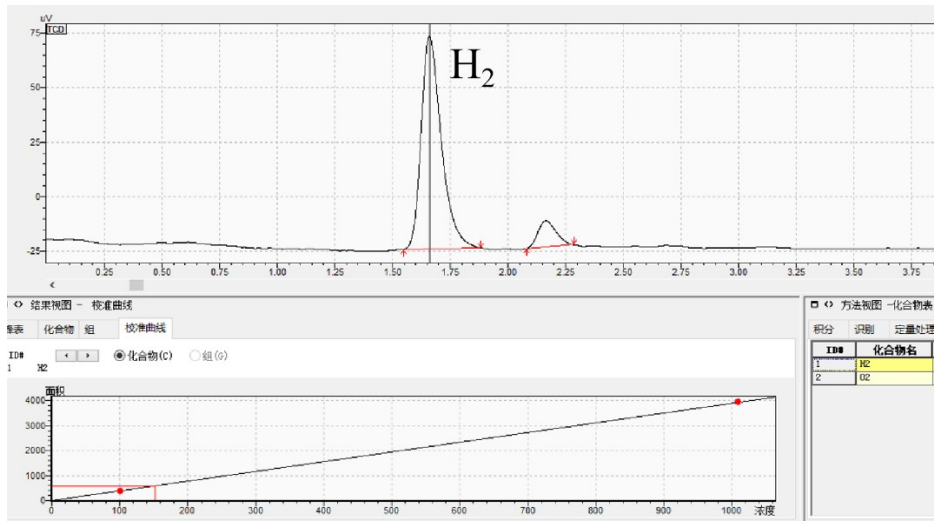


Fig. S10. The calibration curves of H₂, corresponding chromatographic peak.

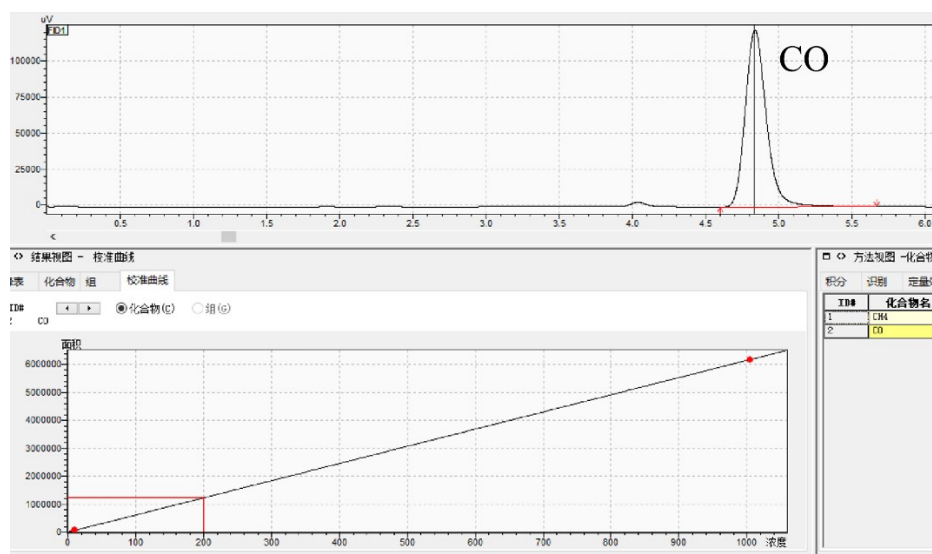


Fig. S11. The calibration curves of CO, corresponding chromatographic peak.

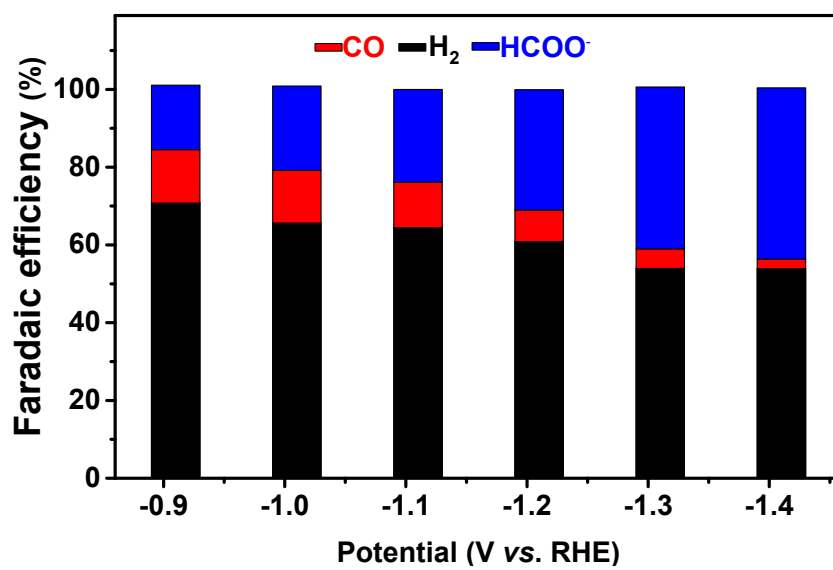


Fig. S12. FEs of CO, H₂ and HCOO⁻ for In@NC.

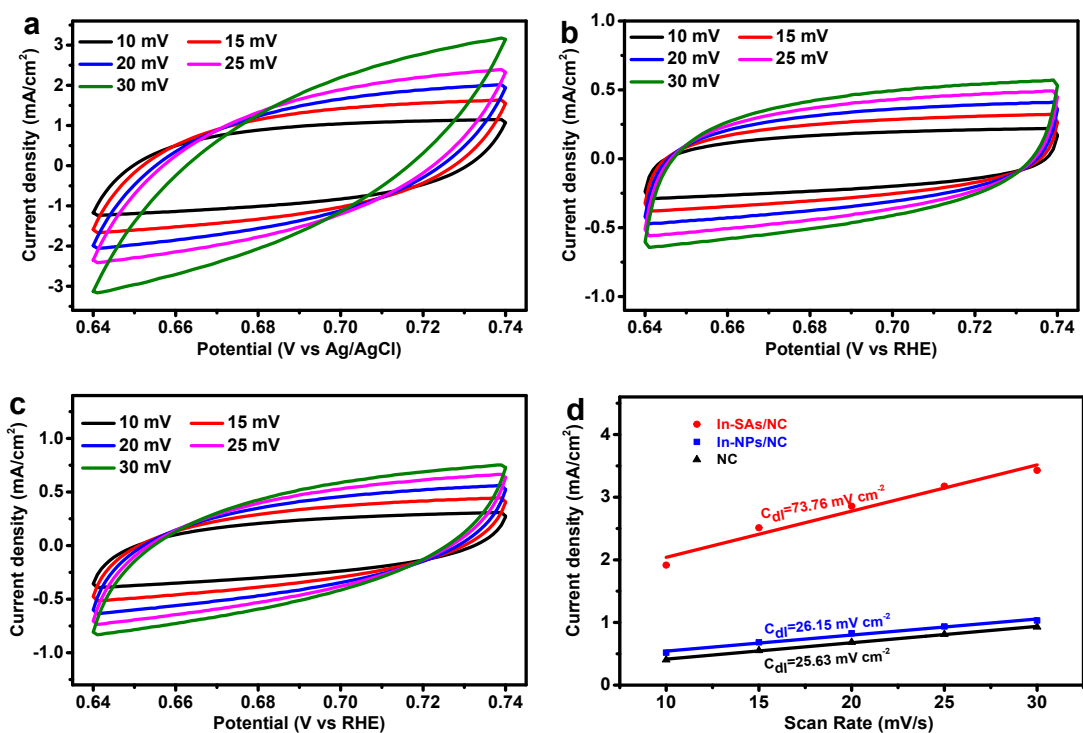


Fig. S13. Electrochemical capacitance measurements of the catalysts with different scan rate. (a) In-SACs, (b) In@NC, (c) NC. (d) Linear fittings of the current density differences (ΔJ) with the scan rates to determine the double layer capacitance (C_{dl}) and electrochemical surface area (ECSA).

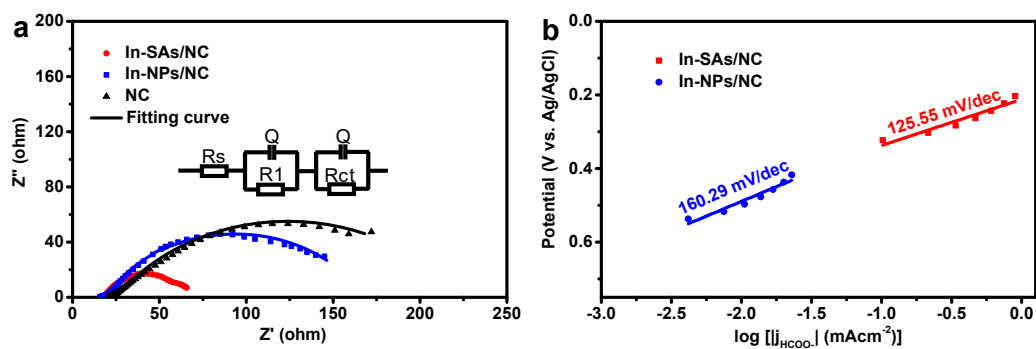


Fig. S14. (a) Nyquist plots for In-SACs, In@NC and NC. (b) Tafel plots of the partial HCOO^- current density for In-SACs and In@NC at different potentials.

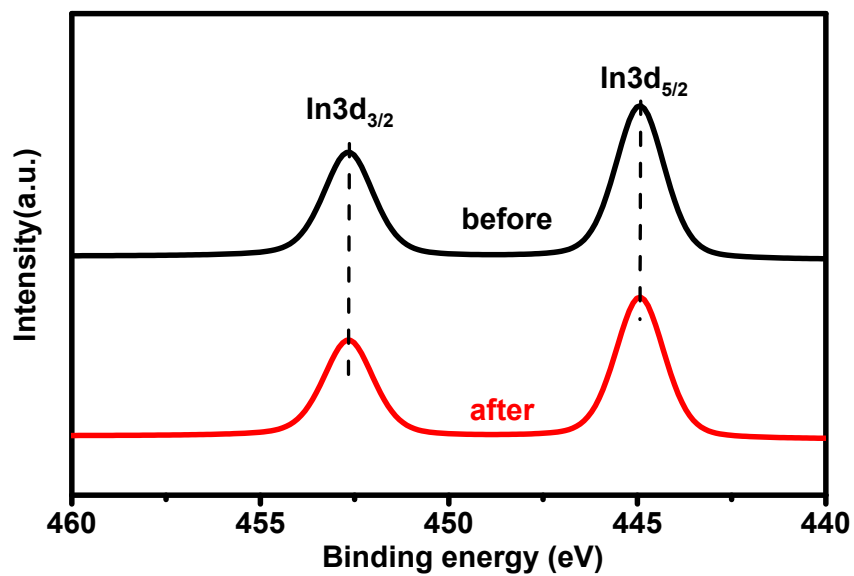


Fig. S15. XPS In 3d spectra of In-SACs obtained before and after electrochemical reduction.

Table S1. Comparative study of electrocatalytic property in literatures.

Materials	Electrolyte	Potential (V vs RHE)	Current density (mA cm⁻²)	Maximum FE (%)	Ref.
Mn-In₂S₃ nanosheets	0.1 M KHCO ₃	-1.2	20.3	86	1
In(OH)₃/C	0.5 M K ₂ SO ₄	-1.1	5.2	77	2
In-Sn alloy	0.1 M KHCO ₃	-1.2	9.6	79	3
In/Carbon	0.1 M K ₂ SO ₄	-1.2	6.1	45	4
In₂O₃-rGO	0.1 M KHCO ₃	-1.2	22.17	84.6	5
In-Cu nanoparticle	0.1 M KHCO ₃	-1.2	4.0	90	6
In-BDC	0.5 M KHCO ₃	-1.069	0.667	80	7
In-N-C	0.5 M KHCO ₃	-0.99	19.5	63	8
In-SAs/NC	0.5 M KHCO ₃	-0.95	29.5	84	9
In single atom	0.5 M KHCO₃	-0.91	38.94	53.98	This work
		-1.01	46.13	61.71	This work
		-1.11	54.52	69	This work
		-1.21	63.21	76.13	This work
		1.31	72.33	85.2	This work
		-1.41	81.08	78.95	This work

1. A. Zhang, Y. Liang, H. Li, X. Zhao, Y. Chen, B. Zhang, W. Zhu and J. Zeng, *Nano Lett*, 2019, **19**, 6547-6553.
2. A. Rabiee and D. Nematollahi, *Materials Chemistry and Physics*, 2017, **193**, 109-116.
3. Q. Lai, N. Yang and G. Yuan, *Electrochemistry Communications*, 2017, **83**, 24-27.
4. Z. Xia, M. Freeman, D. Zhang, B. Yang, L. Lei, Z. Li and Y. Hou, *ChemElectroChem*, 2018, **5**, 253-259.
5. Z. Zhang, F. Ahmad, W. Zhao, W. Yan, W. Zhang, H. Huang, C. Ma and J. Zeng, *Nano Lett*, 2019, **19**, 4029-4034.
6. B. Wei, Y. Xiong, Z. Zhang, J. Hao, L. Li and W. Shi, *Applied Catalysis B: Environmental*, 2021, **283**, 119646.
7. S. Z. Hou, X. D. Zhang, W. W. Yuan, Y. X. Li and Z. Y. Gu, *Inorg Chem*, 2020, **59**, 11298-11304.
8. P. Lu, X. Tan, H. Zhao, Q. Xiang, K. Liu, X. Zhao, X. Yin, X. Li, X. Hai, S. Xi, A. T. S. Wee, S. J. Pennycook, X. Yu, M. Yuan, J. Wu, G. Zhang, S. C. Smith and Z. Yin, *ACS Nano*, 2021, **15**, 5671-5678.
9. H. Shang, T. Wang, J. Pei, Z. Jiang, D. Zhou, Y. Wang, H. Li, J. Dong, Z. Zhuang, W. Chen, D. Wang, J. Zhang and Y. Li, *Angew Chem Int Ed Engl*, 2020, **59**, 22465-22469.